Nasehi Ghashouieh *et al.*
Int J Concr Struct Mater (2024) 18:74
https://doi.org/10.1186/s40069-024-00715-7

International Journal of Concrete Structures and Materials

RESEARCH

Open Access

Microstructural Analysis of the Effect of Using Nano-silica on the Mechanical Properties of Cement–Sand Mortar Under the Effect of Heat

Motahereh Nasehi Ghashouieh[1], Mohsen Malekinejad[1,2*] and Mohammad Amiri[3*]

Abstract

The performance of cement-based materials depends on the characteristics of solid particles at the nano-scale or nanometer porosities in the interfacial transition zone between cement particles and aggregate. Heat significantly affects the properties of these particles and the connection between them. Accordingly, the present study seeks to investigate the effect of nano-silica on the strength parameters of sand–cement mortar at high temperatures. In this regard, the sand–cement mortar was prepared by replacing 5, 10, and 15 percent of cement with nano-silica. The specimens were subjected to temperatures of 25, 100, 200, 400, 600, and 800 °C after curing at the ages of 3, 28, and 90 days. The effect of high temperatures on the physical and mechanical properties of sand–cement mortar was analyzed using macro-structural tests of compressive strength, loss in weight, and water absorption, and microstructural tests of X-ray diffraction (XRD), and scanning electron microscopy (SEM). The results revealed that the macro-structural behavior of sand–cement mortar highly depends on the microstructure and changes in cement nanostructures during heat treatment. Primary portlandite and C–S–H nanostructure were destroyed at 600 °C, and alite, belite, and β-wollastonite were formed at 800 °C. Adding nano-silica improved the strength properties of sand–cement mortar against heat, so the compressive strength of 28-day specimens containing 15% nano-silica increased from 13.9 to 19.2 MPa at a temperature of 800 °C.

Keywords Sand–cement mortar, High-temperature concrete, Cement nanostructures, Nano-silica, Compressive strength

1 Introduction

Concrete and cement-based mortars are constantly affected by several stresses during their operation life. A significant change in the temperature of the environment surrounding concrete under fire conditions or its application in special structures such as nuclear reactors, and chemical storage tanks, which can put concrete under high thermal stresses, can affect the concrete performance (Amiri et al., 2022; Singh et al., 2023). Thermal stresses can affect concrete performance, especially the microstructure of cement paste. Hence, examining the behavior of cement composite under high-temperature conditions can give engineers an appropriate guide to

Journal information: ISSN 1976-0485 / eISSN 2234-1315.

*Correspondence:
Mohsen Malekinejad
malekinejad.mohsen@iau.ac.ir
Mohammad Amiri
amirii@hormozgan.ac.ir
[1] Department of Civil Engineering, Islamic Azad University, Sirjan Branch, Sirjan, Iran
[2] Young Researchers and Elite Club, Islamic Azad University, Sirjan Branch, Sirjan, Iran
[3] Faculty of Engineering, University of Hormozgan, Bandar Abbas, Iran

design resistant structures in certain conditions (Najeeb & Mosaberpanah, 2023).

High heat in concrete can have destructive effects on the concrete microstructure and macrostructure. Heat primarily weakens the mechanical properties and durability of concrete through the release of water from the holes and capillary spaces in the concrete microstructure. High heat can cause a disconnection in the hydrated nanostructures in cement mortar. It also plays a significant role in weakening the bonds between the interfacial transition zones (ITZ). Given the high inter-pore pressure, water release from the chemical bond space in C–S–H makes the concrete destruction at temperatures higher than 450 °C. No significant changes are seen in the mechanical properties of concrete in temperatures between 27 and 100 °C, but a reduction of up to 40% in the values of compressive strength, tensile strength, and modulus of elasticity is seen after applying the temperature of 350 °C in the initial stages (Khan et al., 2022b). A heat between 500 and 900 °C results in crystal changes and destruction in portlandite and cement nanostructures, and the formation of carbonate minerals in the concrete matrix (Elkady et al., 2019).

C–S–H nanostructures are one of the factors that play a key role in creating concrete strength. It is the result of the reaction of water with different phases of calcium silicate (C_2S and C_3S) (Wang et al., 2022). The C–S–H nanostructure, making up 75% of the cement paste particles under the conditions of full hydration in cement composites, is changed and destroyed under high-temperature conditions, resulting in a sharp reduction in the strength of concrete under high thermal stresses (Amiri et al., 2020; de Oliveira et al., 2023). High temperature decomposes hydroxide and water vapor in the C–S–H structure, which finally results in the failure of this structure and its destruction (Mansourghanaei et al., 2022). An appropriate method to improve the performance of concrete in the face of high thermal stresses is using materials that increase the production process and the value of C–S–H nanostructures in the cement composite paste, and increase its strength by creating strong bonds in the microstructures in the cement mortar (Huang et al., 2022). Nano-silica is an active pozzolan and a very effective filler in concrete thanks to the shape and size of its particles. Amorphous (non-crystalline) silica in nano-silica can enter into chemical interactions with hydration products and modify the structure of cement paste (Anto et al., 2022; Mazloom et al., 2021). Nano-silica has a high specific surface and plays a big role in the expansion of hydration products. In addition, nano-silica is effective in creating a regular mortar structure, improving the ITZ and reducing cracks and pore size due to its filler function and the formation of C–S–H (Afzali-Naniz et al., 2024; Nithurshan et al. 2024). It has been reported that using nano-silica in concrete improves compressive strength, flexural strength, modulus of elasticity, and velocity of ultrasonic waves (Abhilash et al., 2021; Abna & Mazloom, 2022; Khan et al., 2022a; Shyamala et al., 2023). These effects improve the performance of concrete against heat. Concrete without additives shows a weaker performance against heat due to the weaker performance of zone ITZ (Anand et al., 2014; Brzozowski et al., 2021; Kanagaraj et al., 2023).

Elkady et. al. (2019) studied how different nano-silica dosages affected the structural behavior of concrete. The findings revealed that using a 4.5% dosage of nano-silica caused a 13.5% rise in the compressive strength after 7 days, compared to the standard group. The study suggested that nano-silica particles agglomerated and prolonged the interaction time with the excess (CH), leading to the creation of CSH gel. Studies of Mukharjee and Barai (2020) have demonstrated that the compressive strength of mortar can be improved by increasing the amount of nano-silica, which improves the matrix. According to the studies of Abna and Mazloom (2022), the addition of nano-silica improves the flexural strength of concrete. The studies of Althoey et. al. (2023) show that around 2–4% of nano-silica in various types of concrete is suitable to improve the influence of nano-silica on the physical, durability, and mechanical properties and densify concrete microstructure. Also, adding nano-silica and fly ash to concrete by forming hydration products including C–S–H and C–A–S–H, and reducing total porosity and pore size helped to increase strength as well as creep and shrinkage properties (Herath et al., 2022).

The study results of Rajamony Laila et. al. (2021) showed that the granite pulver along with the super absorbent polymer increases the compressive strength and flexural strength in comparison with the control mixture. According to the study of Sivakumar and Ananthi (2024), adding vegetable waste biomass ash along with silica sand with an equal replacement up to 10% increased the strength properties in comparison with the control mixture. Paul Thanaraj et al. examined the influence of heating–cooling regime on the engineering properties of structural concrete. The results show that the rate of reduction in tensile and flexural strengths of the concrete was greater than that of compressive strength (Paul Thanaraj et al., 2023). Amiri et al. indicated that replacing 5% of steel slag with cement at 800 °C caused an increase in the compressive strength of the specimens (Amiri et al., 2021). Examining the effect of high temperatures on the properties of cement mortar containing nano-silica revealed a sharp reduction in compressive strength and crack growth, and increased porosity in concrete at temperatures higher than 400 °C (Bastami et al., 2014). In

Table 1 Chemical characteristics of Hormozgan type II Portland cement and nano-silica

Product type	Parameters								
	SiO_2	Al_2O_3	Fe_2O_3	Cao	MgO	K_2O	Na_2O	SO_3	L.O.I
Cement type II	22	5.30	4.00	65.00	2.50	0.70	0.50	2.50	2.50
Nano-silica	96.4	1.32	0.87	0.49	0.97	1.01	0.31	0.10	0.6

a study entitled "Examining the effect of heat on concrete containing fly ash and nano-silica", Mahapatra and Barai showed that specimens containing nano-silica and specimens containing fly ash showed acceptable compressive strength up to a temperature of 400 °C. However, the strength of specimens containing nano-silica decreased when the temperature increased to 600 °C (Mahapatra & Barai, 2019). By examining the mechanical and microscopic properties of concrete containing silica fume and basalt under high temperatures, Yonggui et. al. (2020) showed that basalt and nano-silica fibers improved the performance of the interfacial transition zone (ITZ) and increased the performance of concrete. Kanagaraj et. al. (2023) examined the effect of nanoparticles (nano-silica, nano-cement, nano-fly ash, and nano-metakaolin) on the strength of concrete exposed to heat. The results revealed the positive effect of nanoparticles on the compressive strength of concrete exposed to heat and a reduction in the cracks caused by heat. A review of the literature showed that the effect of nano-silica on the microstructure of concrete and its relationship with the coarse structure has been less stated, especially at high temperatures. Thus, the present study was an attempt to examine the effect of using nano-silica on the mechanical properties of cement–sand mortar under the effect of changes in the cement nanostructures.

2 Materials and Methods

2.1 Materials

Cement, sand, and nano-silica were used to prepare the specimens in the present study. Hormozgan type II Portland cement was used to make all the specimens. Most of the tests in this study were performed based on the ASTM standard (ASTM, 2014).

XRF test was used to evaluate the chemical characteristics of Portland cement and nano-silica, as shown in Table 1. The aggregate used is according to ASTM C136-96 and ASTM C136 standards.

Fig. 1 shows the granulation curve of fine-grained materials. Water absorption of sand is 0.16%, respectively. In this study, the maximum diameter of the used aggregates was 4.75 mm, and the water used in making concrete was the drinking water of Bandar Abbas city with pH = 7.8. The nano-silica was prepared by Armani Shimi Sazeh Company. Table 2 shows the physical characteristics of nano-silica used in this research. All used materials met the requirements in ASTM, DIN, and ACI standards.

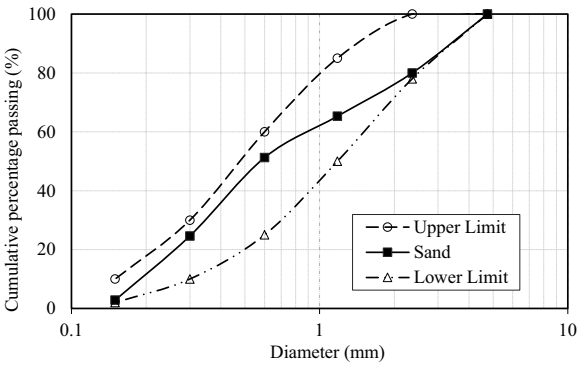

Fig. 1 Granulation curve of the used materials (sand)

Table 2 Some physical characteristics of nano-silica

Physical form	Powder
Specific gravity (kg/m^3)	200–350
Density (kg/cm^3)	2.2–2.35
Special surface area (m^2/g)	193
Particles size (nm)	20–30
Particles shape	Amorphous
Color	Light gray

2.2 Preparation of Tests

Making a concrete sample requires more materials, molds, and equipment. Mortar is used due to the similarity between concrete and mortar. To examine the effect of heat on the microstructure and nanostructure of cement mortar containing nano-silica in the present study, four types of mixing designs were prepared using the ASTM C1384-18e1 standard (ASTM, 2014). Its specifications are presented in Table 3. Mortar was prepared according to the ASTM C109-90 standard. Nano-particles are not easy to disperse uniformly due to their high surface energy. Accordingly, mixing was performed as follows:

The nano-silica particles (with weight percentages of 5, 10, and 15 as a substitute for part of cement) were stirred

Table 3 Specimen mixing design

Number	Mixture	Water: cement (%)	Cement (kg)	Water (kg)	Sand (kg)	Nano-silica (kg)
1	C	0.45	500	225	1375	0
2	C5S	0.45	475	225	1306.25	25
3	C10S	0.45	450	225	1237.5	50
4	C15S	0.45	425	225	1168.75	75

with the mixing water at high speed for 1 min. No superplasticizers were used.

The cement was added to the mixer and mixed at medium speed for another 30 s.

Mixing at medium speed, the sand was added gradually.

The mixture was allowed to rest for 90 s and then mixed at high speed for 1 min. The ratio of water to binder was considered constant and 0.45. The fresh mixture was poured in three layers and with 25 blows into cube molds with dimensions of 50×50×50 mm. After molding, curing has been done for 3, 28, and 90 days in a water pond saturated with lime at a temperature of 23 ± 2 °C. After completing the processing, the specimens of different ages were taken out of the water pool for testing. Before heating, the specimens were dried in the oven at 100 °C for 24 h.

After drying, each specimen was individually placed in an electric furnace at a certain temperature for 2 h. The temperature of the furnace was automatically increased at the rate of 5 °C per minute. After reaching the desired temperature, they were kept at this temperature for 2 h. Then the furnace was turned off and the specimens were cooled in the furnace and removed from the furnace after 24 h. To investigate the effect of temperature on mortar microstructure, mortar stability, and efficiency, to observe the stability of C–S–H and according to previous researches, cement sand mortar specimens were tested under the temperature of 25, 100, 200, 400, 600, and 800 °C. To investigate the changes of C–S–H and compare with previous studies, this temperature range was chosen. The specimen with a temperature of 25 °C was not placed in the oven. Then mechanical tests [loss in weight tests (ASTM C1792-14) and compressive strength (ASTM C39)] and durability test (water absorption test) were performed on the specimens (ASTM, 2014).

2.3 Methodology

The weight of the specimens was measured using a digital scale in two stages (before exposure to heat and after exposure to heat). Then to test the compressive strength, all the specimens were placed under the concrete breaker jack. The compressive strength test of the specimens was performed by the mechanical jack of the Azmoon Company at a speed of 75 kg/s. Finally, the powder obtained from the specimens was collected for SEM and XRD microstructural tests. To prepare X-ray diffraction (XRD) specimens, about 5 g of each specimen was weighed with an accuracy of 0.001 g and they were exposed to radiation with a wavelength of 1.54 Å (related to the kα of Cu element) in the range of 2 to 60 °C. The specimens were tested using an X-ray model (D8-ADVANCE, manufactured by Bruker, Germany) (Moore & Reynolds, 1997). The XRD curve of nano-silica is shown in Fig. 2. The nano-silica used is amorphous and has small amounts of calcite and quartz. To prepare scanning electron microscope (SEM) images of each specimen, 1 g was weighed with an accuracy of 0.001 g. The morphology of the specimens was examined by a model scanning electron microscope (TESCAN vega3) (Ouhadi & Yong, 2003). The SEM image of nano-silica used in the research is shown in Fig. 3.

To perform the water absorption test, after drying in the laboratory environment and weighing (initial dry weight: m_0), the processed specimens were immersed in water for 330 min, 24 h, 48 h, and 72 h. Then they were removed from the water, and their surface was dried with a cloth and then weighed (saturated weight: m_1). The water absorption percentage of the specimens was obtained using Eq. 1.

$$\text{Water absorption } (\%) = 100(m_1 - m_0)/m_0. \quad (1)$$

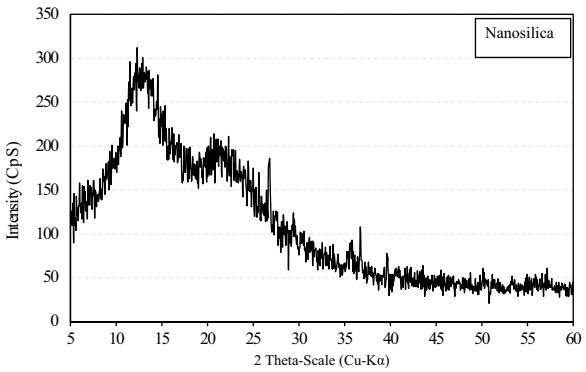

Fig. 2 X-ray diffraction curve of nano-silica

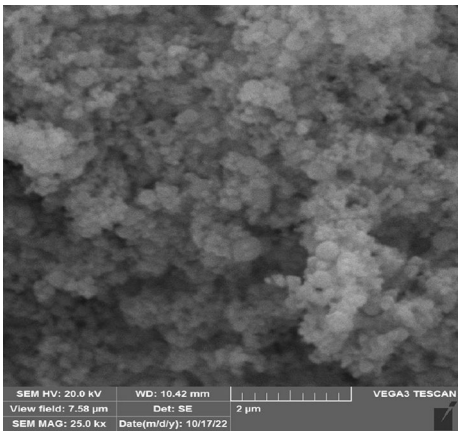

Fig. 3 SEM image of nano-silica

3 Results and Discussion

3.1 X-Ray Diffraction (XRD) Analysis of the Specimens Exposed to Heat

The changes in the X-ray diffraction patterns of specimens without nano-silica and specimens containing 10% nano-silica exposed to heat are as follows.

3.1.1 X-Ray Diffraction (XRD) Analysis of Specimens Without Nano-silica Exposed to Heat

Fig. 4 presents the results of the X-ray diffraction analysis. Crystal phases including quartz (at 4.23 Å and 1.79 Å) (Rosa et al., 2005) and calcite (at 3.83 Å) (Antao & Hassan, 2010), and hydrated phases such as portlandite (at 4.89 Å, 2.6 Å, and 1.9 Å) (Iizuka et al., 2013) and ettringite (at 9.6 Å) (Gatta et al., 2019) are separately observed for the cement–sand mortar at 25 °C.

Based on the results, the primary peak of C–S–H nanostructure (3.02 Å) in specimens with 3, 28, and 90 days of processing is 270 Cp, 343 CpS, and 398 CpS, respectively (Merlino et al., 2000). The intensity of the C–S–H peak has increased with the increase in the age of the specimens due to the progress of the hydration reaction. At the temperature of 800 °C, all peaks such as the C–S–H nanostructure have been removed (Amiri et al., 2022). In the thermal range of 600 °C, alite and belite cement compounds are formed due to C–S–H destruction. β-Wollastonite is formed by increasing the temperature to 800 °C (Rodriguez et al., 2017). The calcite peak (3.8 Å) was observed with an intensity of 36 CpS. Its peak intensity reached 25 CpS as the temperature increased to 800 °C. There were not many changes in

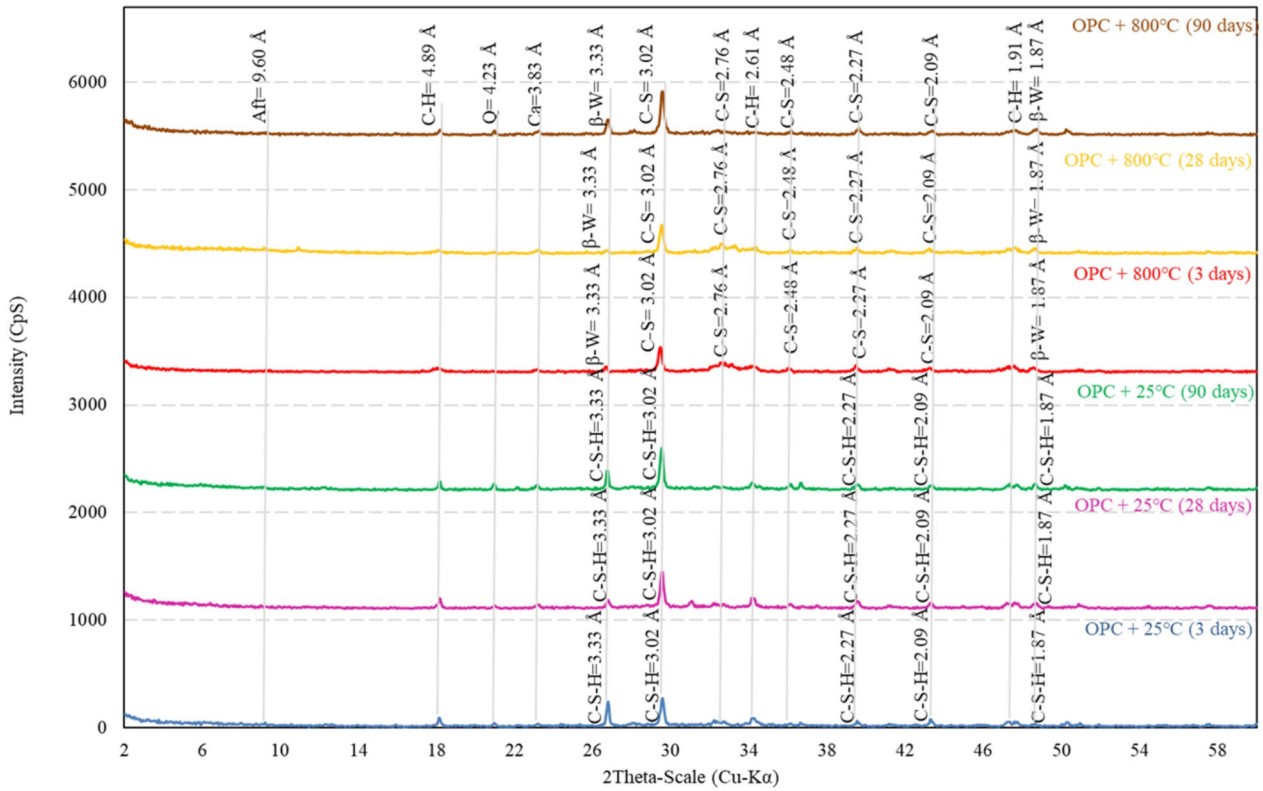

Fig. 4 X-ray diffraction curve of specimens without nano-silica exposed to heat. Aft: ettringite; C_3S: alite; C_2S: belite; C–S–H: calcium silicate hydrate; CH: portlandite; Q: quartz; Ca: calcite; β-W: β-wollastonite

this peak. Portlandite is another dominant product of the cement hydration process. In 3-day, 28-day, and 90-day specimens, the intensity of the biggest peak of portlandite (4.89 Å) is 93 CpS, 102 CpS and 91 CpS, respectively. Portlandite is dehydrated in the thermal range of 450–550 °C and turns to quicklime and water. Portlandite is one of the dominant phases at 800 °C. At a temperature of 600 °C, water released due to dehydration of portlandite in reaction with lime released due to the decomposition of calcium carbonate and primary portlandite led to the formation of secondary portlandite. Due to its formation in critical conditions, secondary portlandite has increased the volume of sand–cement mortar, increased cracks, and, thus, decreased compressive strength (Bodnarova et al., 2013). Alite and belite are formed from the decomposition of C–S–H cement compounds at the temperature of 600 °C. In the 3-day specimen, under the heat of 800 °C, new peaks of calcium silicates of alite and belite were formed at 3.02 Å and 2.27 Å and with the intensity of 238 CpS and 74 CpS, respectively (Tantawy, 2017).

It is difficult to distinguish between alite and belite formed due to heat, and C_3S or C_2S peaks can be used to show both of them (Peng & Huang, 2008). By applying heat of 800 °C, the primary peak of wollastonite resulting from C–S–H decomposition and at 3.33 Å in the 3-day, 28-day, and 90-day specimens, 59 CpS, 40 CpS, and 151 CpS, respectively, were observed.

In the 3-day, 28-day, and 90-day specimens, the peak related to ettringite mineral can be seen at 9.6 Å and with the intensity of 49 CpS, 36 CpS, and 40 CpS. This mineral is formed due to the reaction between sulfate in the pore water of aggregates and cement compounds, and it causes swelling and reduces the durability of concrete. Ettringite is stable up to a temperature of 105 °C and is destroyed by increasing the temperature (Rodriguez et al., 2017). By increasing temperature, the peaks related to quartz decreased and its phase changed at the temperature of 800 °C. Quartz is the lowest-temperature form of silica. α-Quartz transforms into β-quartz at a temperature of 573 °C. This process is reversible up to a temperature of 800 °C, and the volume of quartz increases and micro-cracks appear, and the mechanical properties of the mortar change (Csáki et al., 2018).

3.1.2 X-Ray Diffraction (XRD) Analysis of Specimens Containing 10% Nano-silica Exposed to Heat

Fig. 5 shows the results of the XRD analysis of 90-day specimens containing 10% nano-silica. The peaks of quartz, calcite, C–S–H, portlandite, and ettringite can be seen in the XRD pattern of the 90-day specimen containing 10% nano-silica at a temperature of 25 °C. The comparison between the specimen without nano-silica and the specimen containing 10% nano-silica shows an increase in the number of C–S–H peaks in the specimen containing 10% nano-silica. Nano-silica particles can increase the amount of C–S–H in the mortar matrix by accelerating the hydration process of cement and by consuming CH, thus reducing the amount of portlandite (Khaloo et al., 2016). The primary peak related to the C–S–H nanostructure (3.02 Å) is 430 CpS, which has increased by 8% compared to the specimen without nano-silica. This trend is also true for other C–S–H nanostructured peaks. By increasing the temperature to 200 °C, the intensity of the C–S–H peak increased due to the removal of pore water and the increase of X-ray reflectivity. At temperatures of 600 °C and 800 °C, peaks such as C–S–H have been removed (Zhang et al., 2023). The calcite peak is observed at 3.8 Å with an intensity of 45 CpS. By increasing the temperature to 600 °C, the calcite peak decreases, and at 800 °C, its peak intensity is 28 CpS due to thermal decomposition.

Adding 10% nano-silica caused a decrease in the intensity of the primary portlandite peak (4.89 Å) from 93 to 74 CpS due to the consumption of portlandite during hydration and the increase in C–S–H production. By increasing the temperature to 200 °C, the intensity of the portlandite peak increased due to the removal of surface water, and thus the increase in X-ray reflectivity. Primary portlandite is destroyed at 550 °C and secondary portlandite is observed at 600 °C (Sabeur et al., 2016). At the temperature of 600 °C, alite and belite are formed due to the decomposition of C–S–H. At the temperature of 800 °C, new peaks of alite and belite are formed at 3.02 Å and 2.27 Å with the intensity of 238 CpS and 66 CpS, respectively (Bodnarova et al., 2013). At the temperature of 800 °C, new wollastonite peaks were formed at 3.33, 3.17, and 1.87 Å and with the intensity of 231 CpS, 154 CpS, and 50 CpS. β-Wollastonite is one of the dominant phases of the specimen containing 10% nano-silica. The peaks related to ettringite can be observed at 9.6 and 4.01 Å and with the intensity of 37 CpS and 107 CpS. Ettringite is destroyed at a temperature of 105 °C (Amiri et al., 2023). The interval of 4.23 Å related to the quartz mineral with an intensity of 170 CpS is observed. By increasing the temperature, the peak related to quartz was reduced. At 800 °C, α-quartz has changed phase to β-quartz (Amiri et al., 2023).

At a temperature of 25 °C, the amount of CH is reduced owing to adding nano-silica, and the C–S–H nanostructure is the dominant phase. By increasing the temperature to 200 °C, ettringite is destroyed. Alite and belite form the dominant phase of the mortar matrix at the temperature of 600 °C simultaneously with the destruction of CH and C–S–H. By increasing the temperature to 800 °C, the mortar matrix includes alite, belite, and β-wollastonite cement compounds. Small amounts of

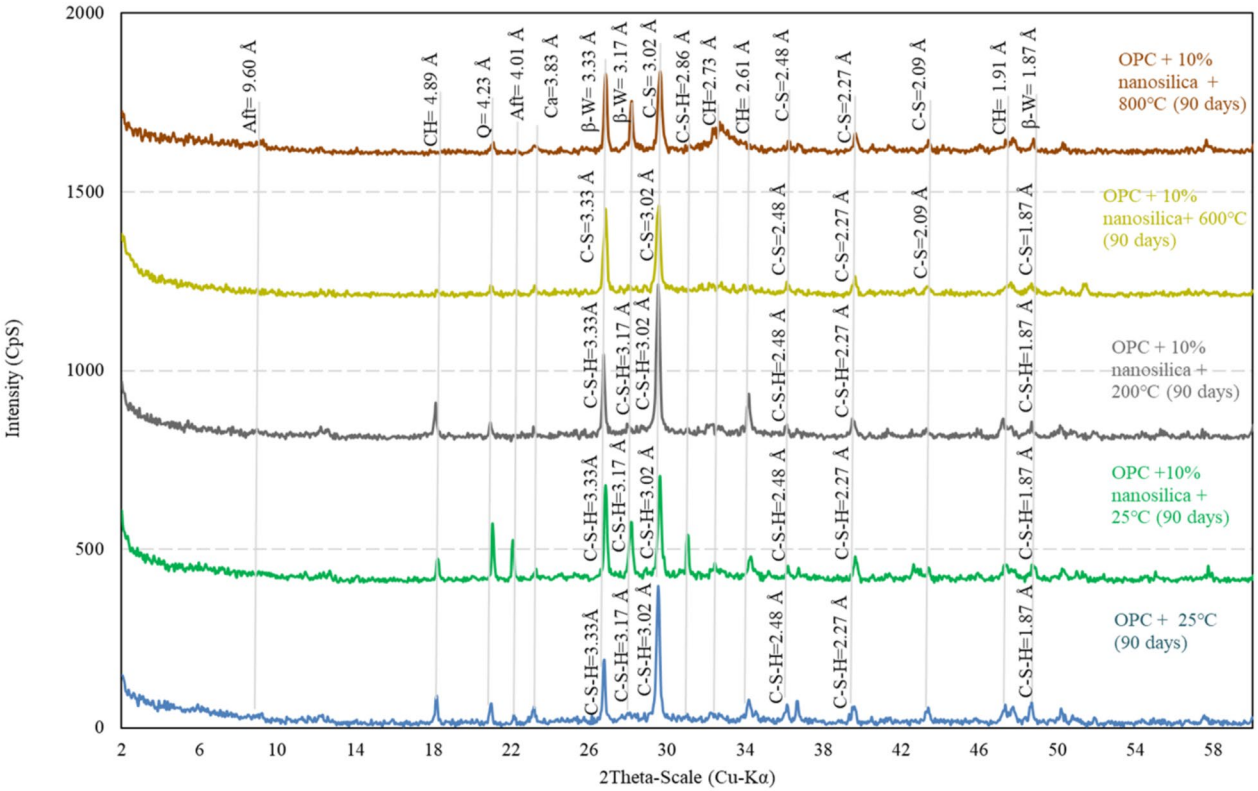

Fig. 5 X-ray diffraction curve of specimens containing 10% nano-silica exposed to heat. Aft: ettringite; C_3S: alite; C_2S: belite; C–S–H: calcium silicate hydrate; CH: portlandite; Q: quartz; Ca: calcite; β-W: β-wollastonite

secondary portlandite and residual calcite were also observed. Comparing the specimen without nano-silica and the specimen containing nano-silica shows the positive effect of nano-silica in reducing the destructive effects of heat due to the reduction of CH and the increase of C–S–H in the mortar matrix (Figs. 6, 7).

3.2 Morphology of the Specimens Exposed to Heat

Fig. 8 illustrates the scanning electron microscope images of 90-day specimens exposed to different temperatures. According to the presented images, portlandite (CH) structures and C–S–H nanostructures can be observed. Fig. 8a shows the specimen without nano-silica at the temperature of 25 °C. At ambient temperature, the sand–cement mortar matrix is relatively compact, the calcium hydroxide crystals are hexagonal, the C–S–H nanostructure is relatively irregular, and its size and value are small. White calcite particles can also be observed in this regard. The mortar matrix is sticky and has a small number of micro-cracks. The needle-shaped structure of ettringite can be also observed. The specimen containing 10% nano-silica at 25 °C can be seen in Fig. 8b. The specimen containing nano-silica has a more uniform texture than the specimen without nano-silica (Fig. 8a). In the specimen containing 10% nano-silica, pores and the needle-shaped structure of ettringite have been significantly reduced. According to the results of X-ray diffraction, nano-silica particles can increase the production of C–S–H cement nanostructure by accelerating the cement hydration process by reacting with portlandite crystals, which reduces the size and value of CH crystals (Khaloo et al., 2016). C–S–H cement nanostructures are placed on top of each other and overlap. As a result, they improve the performance by increasing the density of the sand–cement mortar matrix.

Fig. 8c, d, respectively, illustrates the specimen without nano-silica and the specimen containing 10% nano-silica at a temperature of 200 °C. Capillary water and absorbed water evaporate, and ettringite is decomposed in the thermal range of 25 °C to 100 °C. CH crystals and C–S–H nanostructure remain intact. Due to the evaporation of water in the holes and chemical bonds of the C–S–H nanostructure, it can be observed more clearly. White calcite particles also maintain their stability at 200 °C. The comparison of Fig. 8c, d shows the more cohesive texture of the specimen containing 10% compared to the specimen without nano-silica. The mortar texture was damaged as the temperature increased.

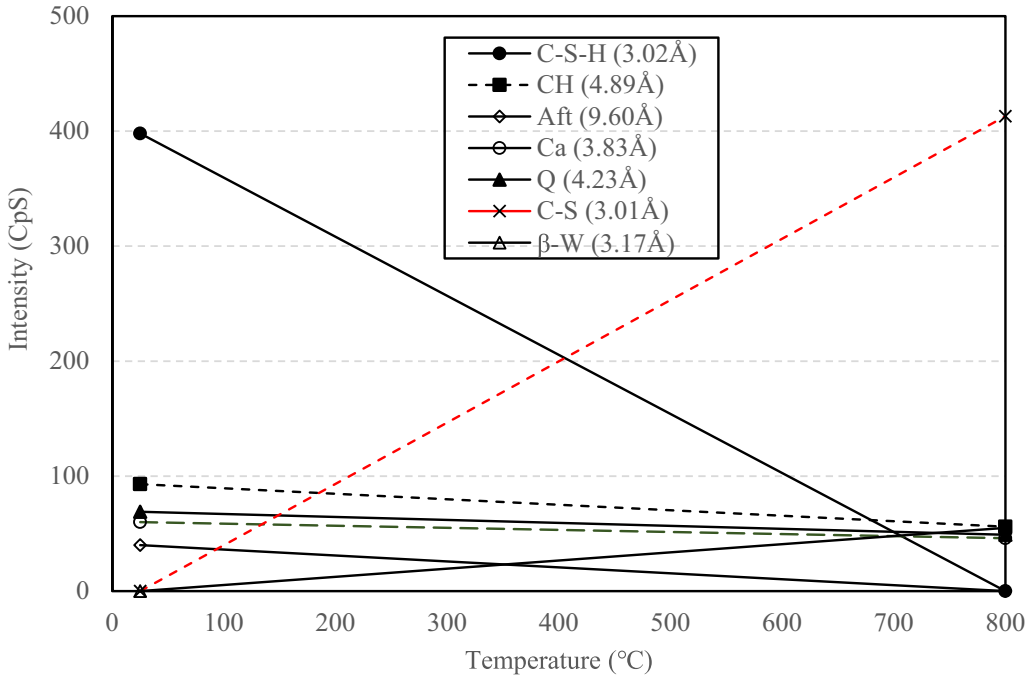

Fig. 6 The curve of the intensity of the peaks of crystal structures in specimens without nano-silica exposed to heat based on XRD analysis

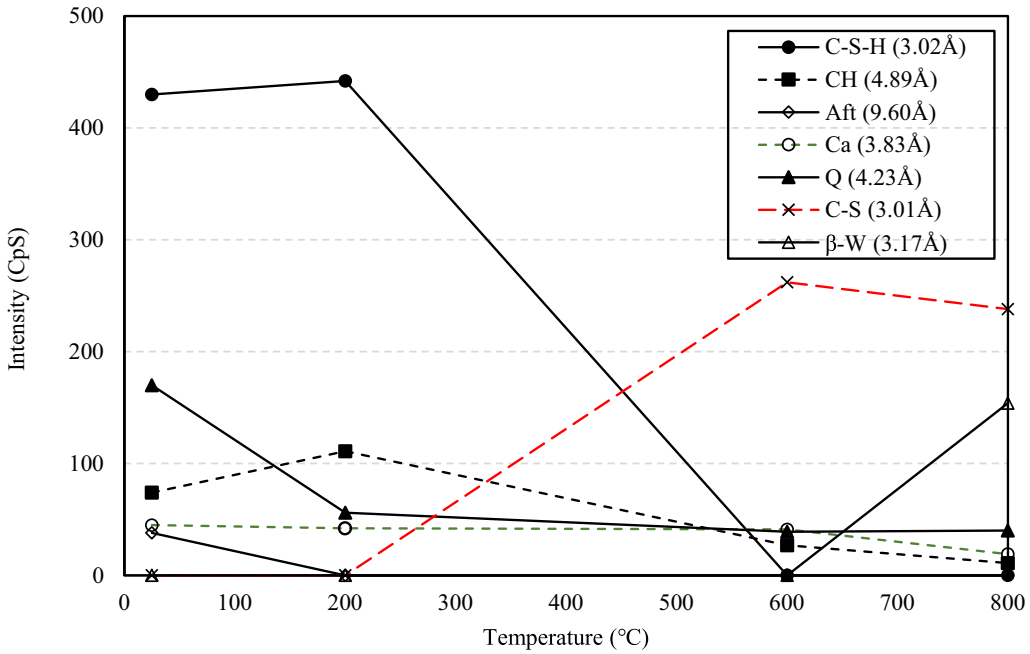

Fig. 7 The curve of the intensity of the peaks of crystal structures in the specimens containing 10% nano-silica exposed to heat based on XRD analysis

The mortar matrix has changed from compact form to porous form. In other words, the space between the mortar matrix increased gradually and the mortar texture cohesion decreased. Fig. 8e, f, respectively, shows the specimen without nano-silica and the specimen containing 10% nano-silica under the temperature

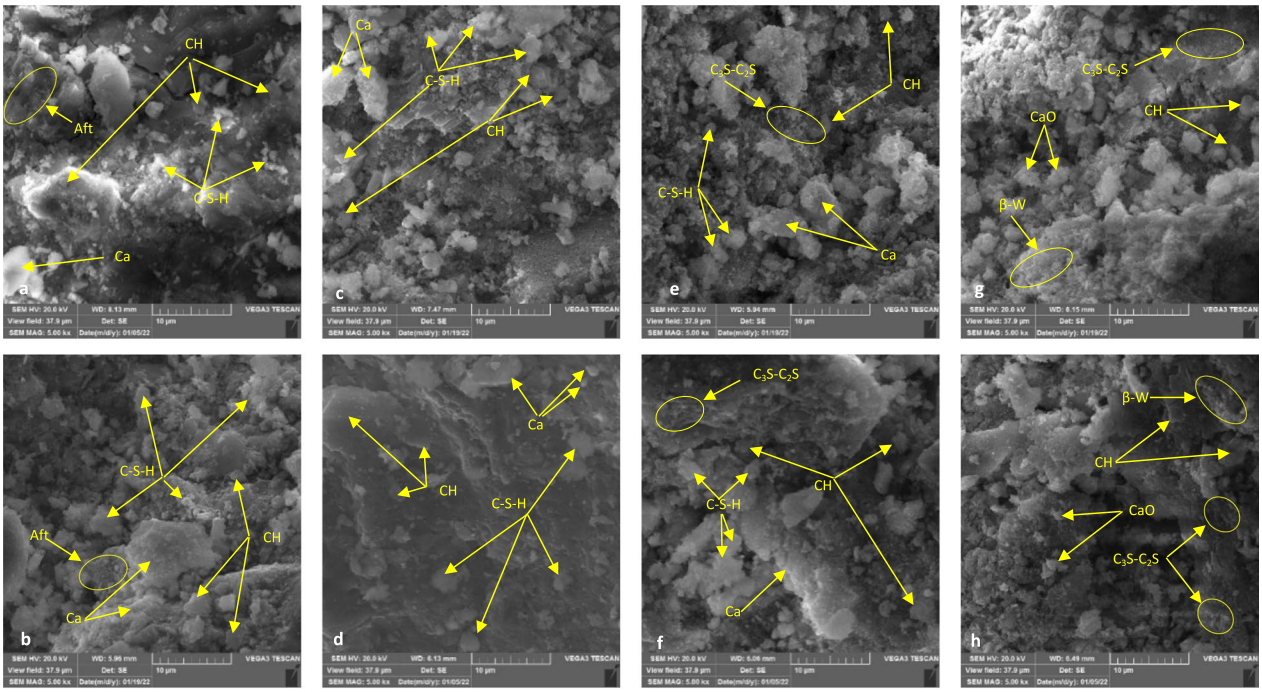

Fig. 8 SEM images of 90-day specimens: **a** specimen C at ambient temperature, **b** specimen C10S at ambient temperature, **c** specimen C at 200 °C, **d** specimen C10S at 200 °C, **e** test C under a temperature of 600 °C, **f** test C10S under a temperature of 600 °C, **g** test C under a temperature of 800 °C, and **h** test C10S under a temperature of 800 °C

of 600 °C. After increasing the temperature to 600 °C, most of the products of the cement hydration process were decomposed, the connections between particles were greatly weakened, and the mortar structure was highly fragmented and became porous.

A major part of the C–S–H cement nanostructure was destroyed by turning into alite and belite, and its network and cohesive structure were destroyed. A large amount of primary portlandite crystals were decomposed. Destruction of primary portlandite is associated with the release of some water and the formation of quicklime. The water released due to the dehydration of portlandite in the reaction with lime released due to the decomposition of calcium carbonate caused the formation of secondary portlandite, which has a weak structure. In other words, the regular layered structure of primary portlandite is completely lost and the weak structure of secondary portlandite is observed. Alite and belite crystals, formed by the decomposition of portlandite, have caused cracks and pores in the mortar matrix. The regular and complete layered structure has been lost (Rodriguez et al., 2017). The mortar matrix expanded and the size of the particles increased, and the connection between them decreased due to the thermal decomposition of cement hydration products.

The comparison of Fig. 8e, f indicates that the specimen containing 10% has better performance against heat and adding nano-silica reduced the destructive effects of heat. Fig. 8g, h, respectively, shows the specimen without nano-silica and under the temperature of 800 °C. As shown in both figures, the regular structure of primary portlandite and C–S–H cement nanostructure has been destroyed. Due to the destruction of primary portlandite, CaO particles are observed. In addition, the irregular and weak structure of secondary portlandite is observed. Based on the X-ray diffraction results, at 800 °C, the dominant phase of the specimen without nano-silica and the specimen containing 10% of nano-silica is calcium silicates alite and belite (resulting from C–S–H destruction and primary portlandite) and the rod-shaped structure of β-wollastonite resulting from C–S–H decomposition (Raheem et al., 2021; Rodriguez et al., 2017). The mortar matrix changed to a glassy structure at a high temperature, the porosity increased with the formation of new structures.

3.3 Changes in the Compressive Strength of the Specimens Exposed to Heat

Fig. 9 shows the compressive strength diagram of sand–cement mortar specimens containing 0%, 5%, 10%, and

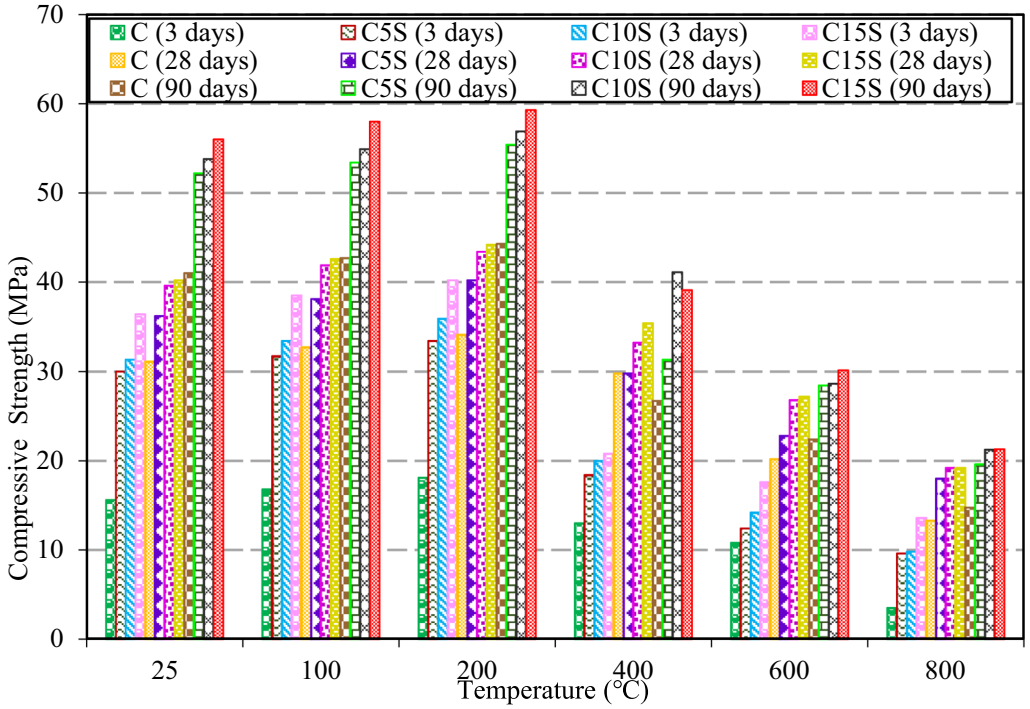

Fig. 9 The changes in the compressive strength of the specimens exposed to heat

15% nano-silica under temperatures of 25 °C to 800 °C during the 3-day, 28-day, and 90-day processing. The 28-day compressive strength of the specimen without nano-silica is 31.1 MPa. By adding 5%, it increased by 16% to 36.2 MPa. The compressive strength of all specimens increased as the nano-silica percentage and the age of the specimens increased, so the highest strength belonged to the specimen containing 15% nano-silica with 56 MPa. Nano-silica particles increase the production of C–S–H cement nanostructure in a reaction with portlandite (CH) crystals by accelerating the cement hydration process (Abreu et al., 2017). The compressive strength of the C–S–H cement nanostructure is higher than that of CH crystals, which is one of the reasons for increasing the compressive strength of specimens containing nano-silica. The compressive strength of the specimens increases by increasing the amount of nano-silica (Mukharjee & Barai, 2014; Zhang et al., 2023).

The 28-day compressive strength of the specimens containing 0%, 5%, 10%, and 15% nano-silica, respectively, increased from 31.1 MPa, 36.2 MPa, 39.6 MPa, and 40.2 MPa at normal temperature to 32.7 MPa, 38.1 MPa, 41.9 MPa, and 42.6 MPa by increasing the temperature to 100 °C. A similar trend was also observed for the compressive strength of the specimens under the temperature of 200 °C. By increasing temperature, compressive strength also increased due to the drying of the specimens and the dehydration of the surface water. By increasing the temperature to 400 °C, the compressive strength of the specimens decreased sharply, so the 28-day compressive strength of the sand-cement mortar specimens containing 0% and 15% nano-silica decreased to 29.8 MPa and 35.4 MPa. The primary portlandite was destroyed at 400 to 550 °C and turned into water and quicklime. Also, the dehydration of C–S–H started at 200 °C and occurred at a more intense rate at 400 °C. Thus, a large part of the C–S–H nanostructure was destroyed due to the increase in irregularities and dehydration at 400 °C (Elkady et al., 2019).

Based on the SEM images, the space between the mortar matrixes increased, and the cohesion of the mortar texture and the compressive strength of the specimens decreased at 400 °C. The compressive strength of specimens containing nano-silica is higher than the specimen without nano-silica at a temperature of 400 °C. Nano-silica reduced the destructive effects of heat by creating a cohesive texture and increasing the density of the sand-cement mortar matrix (Sadrmomtazi et al., 2020). By increasing the temperature to 600 °C, most of the products of the cement hydration process were decomposed and the connections between the particles became very weak. Also, based on the SEM images, the structure of the mortar was strongly fragmented and became porous. At a

temperature of 800 °C, the 28-day compressive strength of specimens without nano-silica and containing 15% was 13.3 MPa and 19.2 MPa, respectively, indicating a decrease of 57% and 52% compared to normal temperature (Amiri et al., 2022). At a temperature range of 600 °C to 800 °C, the calcite in the mortar turned to calcium oxide by releasing CO_2 gas, resulting in more porosity of the specimens and increased cracks in the mortar matrix (Amiri et al., 2023).

The porosity created due to the destruction of C–S–H and primary portlandite and the decomposition of calcite in the mortar caused an expansion in the cracks and the destruction of the interfacial transition zone between the aggregate and the cement paste, and, thus, reduced compressive strength of the specimens. Based on the SEM images, adding nano-silica made the mortar matrix more cohesive and reduced the destructive effects of heat. In almost all temperatures (25 °C to 800 °C), the highest amount of compressive strength was observed in specimens containing 15% nano-silica. Nano-silica increases the strength and durability of concrete at high temperatures by consuming Ca $(OH)_2$ and converting it into a C–S–H cement nanostructure. It causes the growth of long and thin C–S–H nanostructures by occupying less space in the concrete matrix at higher temperatures, leading to microstructure compaction and a reduction in micro-cracks during thermal stresses (Anto et al., 2022).

3.4 Weight Changes of the Specimens Exposed to Heat

Fig. 10 illustrates the loss in weight of the specimens under different temperatures. At a temperature of 100 °C, the normal sand–cement mortar specimen showed the lowest loss in weight and the specimen containing 5% nano-silica showed the highest loss in weight. The loss in weight of these specimens was 1.5% and 2.9%, respectively. At a temperature of 100 °C, free water was released from concrete and caused a loss in weight. By increasing the temperature to 200 °C, the loss in weight of specimens containing 0, 5, 10, and 15% nano-silica due to the destruction of ettringite was 1.7%, 3.4%, 2.8%, and 3.9%, respectively (Aly et al., 2012). By increasing the temperature to 400 °C, the loss in weight of the specimen without nano-silica was 4.7%. By adding 5%, 10%, and 15% nano-silica, the loss in weight values increased slightly to 5.6%, 5.5%, and 6.5%.

By increasing temperature, the C–S–H nanostructure was destructed gradually, which affected the loss in weight and compressive strength of the specimens. The process of dihydroxylation and the release of hydroxyl ions in the form of water from the mortar tissue was another factor of loss in weight in the temperature range of 400 °C to 600 °C (Amiri et al., 2022). By increasing the temperature to 600 °C, the loss in weight of the specimens containing 0, 5, 10, and 15% nano-silica due to the decomposition of portlandite and C–S–H and C–A–S–H nanostructures was reported at 6.42%, 7.2%, 6.6%, and

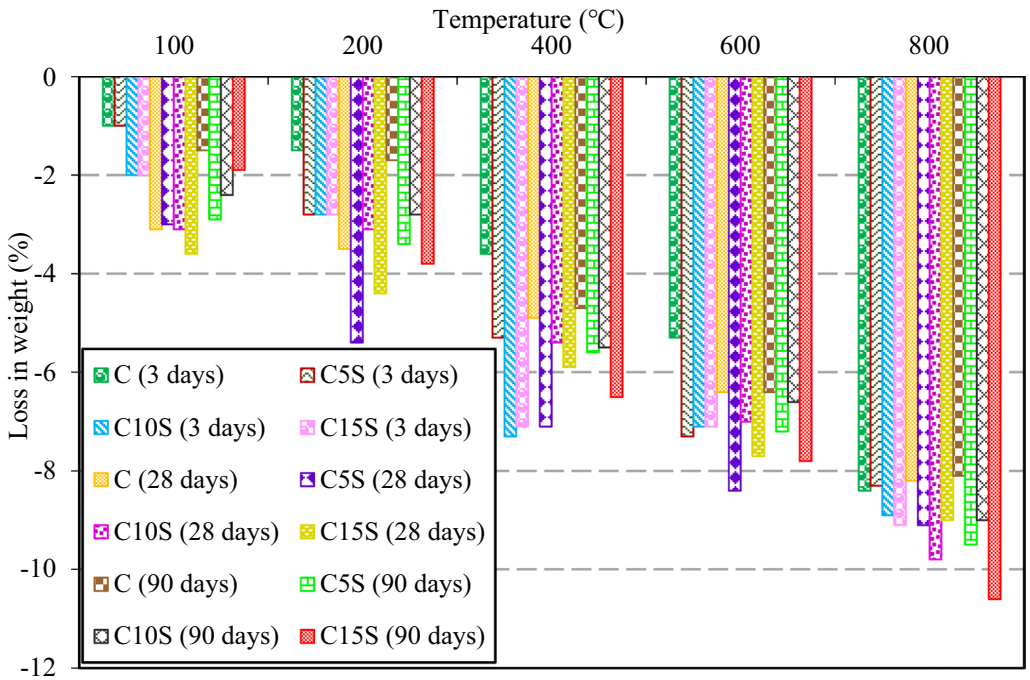

Fig. 10 The weight changes in the specimens exposed to heat

7.8%, respectively (Rodriguez-Navarro et al., 2009). The high loss in weight led to the creation of micro-cracks in the mortar structure and, thus, reduced compressive strength. The results of the loss in weight are in line with SEM images, XRD curves, and compressive strength changes (Fig. 9). Due to the decomposition of calcium carbonate, the loss in weight of the specimens at the temperature of 800 °C reached its maximum value. The loss in weight of specimens containing 0, 5, 10, and 15% nano-silica was reported at 8.1%, 9.5%, 9%, and 10.6%, respectively (Bodnarova et al., 2013).

Due to its high surface area, nano-silica absorbs some water, so the weight loss of specimens with nano-silica is greater. In addition, the specimens with nano-silica have more hydrates and subsequently their weight loss may be greater. The factor of loss in weight in the specimens includes dehydration and destruction of ettringite (temperature 100–200 °C), decomposition of C–S–H and dihydroxylation (temperature 600–400 °C), destruction of portlandite and C–S–H (temperature 600 °C), and the decomposition of calcium carbonate (temperature 800 °C) (de Oliveira et al., 2023).

Table 4 28-day water absorption of all specimens

Mixture	Water absorption (30 min)	Water absorption (24 h)	Water absorption (48 h)	Water absorption (72 h)
C	4.51%	5.27%	5.33%	5.37%
C5S	4.16%	4.86%	4.94%	4.96%
C10S	3.8%	4.22%	4.29%	4.37%
C15S	2.90%	3.28%	3.31%	3.35%

3.5 Changes in Water Absorption of the Specimens

Water absorption is one of the characteristics of concrete, which indicates the characteristics of its microstructure in terms of pores and their connection. Most of the destructive reactions that occur in concrete over time are due to water penetration. Water is always a factor that initiates or accelerates destructive reactions in concrete.

In the present study, the water absorption percentage on 28-day specimens was determined based on the ASTM C642 standard. Table 4 and Fig. 11 shows the results of the water absorption test on all the specimens over time. The amount of water absorption by the specimens decreases by adding nano-silica, so the water absorption of the specimen without nano-silica increased to 5.37% after 72 h of immersing in water and by 3.35% adding 15% nano-silica. Adding nano-silica reduced the water absorption of the specimens. According to the microstructural results of XRD and SEM images and

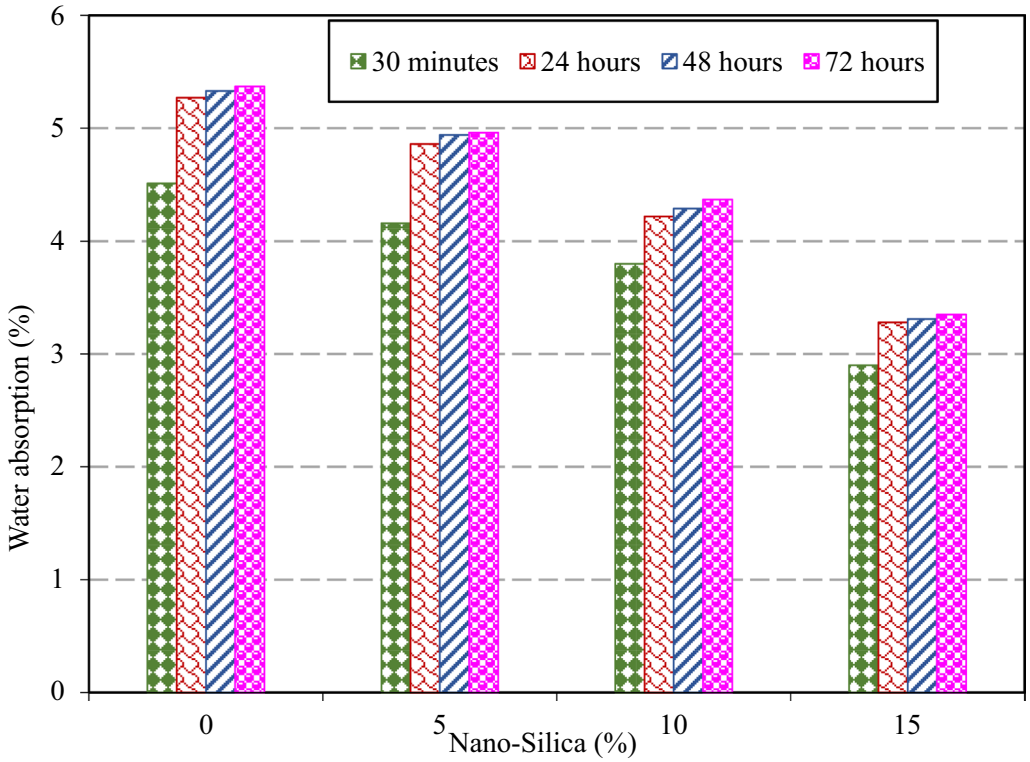

Fig. 11 The water absorption of specimens

compressive strength results, the primary reason for a reduction in the water absorption of the specimens is the increase of C–S–H in the mortar and the nano-silica filler performance (Abhilash et al., 2021). Table 4 shows the effect of nano-silica on the water absorption of specimens over time. The amount of water absorption of the specimens also increased over time. However, the rate of this increase in specimens containing nano-silica was lower than in the control specimen.

4 Conclusion

The present study examined the effect of nano-silica on the engineering properties of sand-cement mortar exposed to heat from a microstructural point of view. Its significant results are presented below.

- By adding nano-silica to cement, the amount of CH crystals in the matrix decreased and the amount of C–S–H nanostructure increased. Given the better performance of C–S–H compared to CH when exposed to temperature, the better performance of specimens containing nano-silica was observed at 400 °C
- Nano-silica particles caused the production and expansion of C–S–H through continuous reaction with CH crystals, which helps to improve the hydration speed of cement and the content of C–S–H nanostructure.
- Adding nano-silica to mortar increased the thermal stability of concrete and reduced the heat loss of the specimens. Its primary reason is the need for a higher temperature for the decomposition of the nanostructures formed in the mortar matrix.
- The drop in the strength at the temperature range of 400 °C to 600 °C is less for the specimens containing nano-silica, due to the pozzolanic property of nano-silica and reaction with CH and thus increasing C–S–H in the specimens, so at a temperature 800 °C, 28-day strength of the specimen without nano-silica and the specimen containing 10% nano-silica is 13.3 MPa and 19.2 MPa, respectively.
- The amount of water absorption by the specimens decreased by adding nano-silica, and this decrease reached its maximum level in the specimens containing 5%. The primary reason for this is the nano-silica filler performance.
- The phase change of α-quartz to β-quartz due to heat has led to a change in the engineering properties of mortar, including increased porosity and water absorption at a temperature of 800 °C.
- According to the SEM images, adding nano-silica made the mortar matrix more cohesive and reduced the destructive effects of heat.
- SEM analysis of the specimens heated at 600 °C and 800 °C indicates the formation of secondary portlandite. Secondary portlandite is formed due to the reaction of water (resulting from dehydration and destruction of primary portlandite) with CaO (resulting from the decomposition of calcite). Secondary portlandite has a weak structure.

5 Recommendations for Future Research

Investigate the impact of cooling and heating cycles on the properties of cement-sand mortar containing nano-silica.
Examine how different heating rates affect the properties of cement-sand mortar containing nano-silica.
Explore the combined effect of nano-silica and other additives, such as fly ash, on the properties of concrete exposed to heat.

Author contributions
Motahereh Nasehi Ghashouieh: review and editing; investigation, resources, formal analysis, methodology. Mohsen Malekinejad: visualization, investigation. Mohammad Amiri: conceptualization, methodology, validation, formal analysis, writing—review and editing, supervision, writing.

Availability of data and materials
The datasets generated during and/or analyzed during the current study are available from the corresponding author on reasonable request.

Declarations

Ethics approval and consent to participate
Corresponding authors on behalf of all the authors assure that this manuscript was not submitted to another journal at the same time. All authors agree to publish the article.

Consent for publication
All authors agree to publish the article.

Competing interests
The authors declare that they have no conflict of interest.

Received: 10 January 2024 Accepted: 27 July 2024
Published online: 25 October 2024

References

Abhilash, P., Nayak, D. K., Sangoju, B., Kumar, R., & Kumar, V. (2021). Effect of nano-silica in concrete; a review. *Construction and Building Materials, 278*, 122347. https://doi.org/10.1016/j.conbuildmat.2021.122347
Abna, A., & Mazloom, M. (2022). Flexural properties of fiber reinforced concrete containing silica fume and nano-silica. *Materials Letters, 316*, 132003. https://doi.org/10.1016/j.matlet.2022.132003
Abreu, G. B. D., Costa, S. M. M., Gumieri, A. G., Calixto, J. M. F., França, F. C., Silva, C., & Quinões, A. D. (2017). Mechanical properties and microstructure of high performance concrete containing stabilized nano-silica. *Matéria*

(Rio de Janeiro), 22, e11824. https://doi.org/10.1590/S1517-707620170002.0156

Afzali-Naniz, O., Mazloom, M., & Karamloo, M. (2021). Effect of nano and micro SiO_2 on brittleness and fracture parameters of self-compacting lightweight concrete. *Construction and Building Materials, 299*, 124354. https://doi.org/10.1016/j.conbuildmat.2021.124354

Althoey, F., Zaid, O., Martínez-García, R., Alsharari, F., Ahmed, M., & Arbili, M. M. (2023). Impact of nano-silica on the hydration, strength, durability, and microstructural properties of concrete: A state-of-the-art review. *Case Studies in Construction Materials, 18*, e01997. https://doi.org/10.1016/j.cscm.2023.e01997

Aly, M., Hashmi, M., Olabi, A., Messeiry, M., Abadir, E., & Hussain, A. (2012). Effect of colloidal nano-silica on the mechanical and physical behaviour of waste-glass cement mortar. *Materials & Design, 33*, 127–135. https://doi.org/10.1016/j.matdes.2011.07.008

Amiri, M., Aryanpour, M., & Porhonar, F. (2022). Microstructural study of concrete performance after exposure to elevated temperatures via considering C–S–H nanostructure changes. *High Temperature Materials and Processes, 41*, 224–237. https://doi.org/10.1515/htmp-2022-0030

Amiri, M., Arzanian Karamallah, K., & Aryanpoor, M. (2020). Efficacy of elevated temperatures on mechanical properties of concrete containing aluminum slag from the microstructural perspective. *Concrete Research Quartery Journal University of Guilan (Iran), 13*, 19–32. https://doi.org/10.22124/jcr.2020.15566.1421

Amiri, M., Kalantari, B., & Porhonar, F. (2023). The effect of thermal stabilization process on mineralogy, morphology and engineering properties of red soil in southern Iran. *Case Studies in Construction Materials*. https://doi.org/10.1016/j.cscm.2023.e02454

Amiri, M., Vatanpour Aghjeh Mashhad, A., Aryanpour, M., & Ghasemi, S. (2021). Studying the mechanical properties and microstructure of concrete containing steel slang exposed to high temperature. *Concrete Research Quartery Journal of Guilan University of Iran, 14*, 21–35. https://doi.org/10.22124/jcr.2021.17796.1457

Anand, N., Arulraj, G., & Aravindhan, C. (2014). Stress-strain behaviour of normal compacting and self compacting concrete under elevated temperatures. *Journal of Structural Fire Engineering, 5*, 63–76. https://doi.org/10.1260/2040-2317.5.1.63

Antao, S. M., & Hassan, I. (2010). Temperature dependence of the structural parameters in the transformation of aragonite to calcite, as determined from in situ synchrotron powder X-ray-diffraction data. *The Canadian Mineralogist, 48*, 1225–1236. https://doi.org/10.3749/canmin.48.5.1225

Anto, G., Athira, K., Nair, N. A., Sai, T. Y., Yadav, A. L., & Sairam, V. (2022). Mechanical properties and durability of ternary blended cement paste containing rice husk ash and nano silica. *Construction and Building Materials, 342*, 127732. https://doi.org/10.1016/j.conbuildmat.2022.127732

ASTM. (2014). Annual book of ASTM standards. American Society for Testing & Materials America. https://www.astm.org

Bastami, M., Baghbadrani, M., & Aslani, F. (2014). Performance of nano-silica modified high strength concrete at elevated temperatures. *Construction and Building Materials, 68*, 402–408. https://doi.org/10.1016/j.conbuildmat.2014.06.026

Bodnarova, L., Valek, J., Sitek, L., & Foldyna, J. (2013). Effect of high temperatures on cement composite materials in concrete structures. *Acta Geodynamica et Geomaterialia, 10*, 173–180. https://doi.org/10.13168/AGG.2013.0017

Brzozowski, P., Strzałkowski, J., Rychtowski, P., Wróbel, R., Tryba, B., & Horszczaruk, E. (2021). Effect of nano-SiO_2 on the microstructure and mechanical properties of concrete under high temperature conditions. *Materials, 15*, 166. https://doi.org/10.3390/ma15010166

Csáki, Š, Ondruška, J., Trnovcova, V., Štubňa, I., Dobroň, P., & Vozár, L. (2018). Temperature dependence of the AC conductivity of illitic clay. *Applied Clay Science, 157*, 19–23. https://doi.org/10.1016/j.clay.2018.02.026

de Oliveira, A. M., Oliveira, A. P., Vieira, J. D., Junior, A. N., & Cascudo, O. (2023). Study of the development of hydration of ternary cement pastes using X-ray computed microtomography, XRD-Rietveld method, TG/DTG, DSC, calorimetry and FTIR techniques. *Journal of Building Engineering, 64*, 105616. https://doi.org/10.1016/j.jobe.2022.105616

Elkady, H. M., Yasien, A. M., Elfeky, M. S., & Serag, M. E. (2019). Assessment of mechanical strength of nano silica concrete (NSC) subjected to elevated temperatures. *Journal of Structural Fire Engineering*. https://doi.org/10.1108/JSFE-10-2017-0041

Gatta, G. D., Hålenius, U., Bosi, F., Cañadillas-Delgado, L., & Fernandez-Diaz, M. T. (2019). Minerals in cement chemistry: A single-crystal neutron diffraction study of ettringite, $Ca_6Al_2(SO_4)_3(OH)_{12}{\cdot}27H_2O$. *American Mineralogist, 104*, 73–78. https://doi.org/10.2138/am-2019-6783

Herath, C., Gunasekara, C., Law, D. W., & Setunge, S. (2022). Long term creep and shrinkage of nano silica modified high volume fly ash concrete. *Journal of Sustainable Cement-Based Materials, 11*, 202–222. https://doi.org/10.1080/21650373.2021.1913660

Huang, J., Zhou, Y., Yang, X., Dong, Y., Jin, M., & Liu, J. (2022). A multi-scale study of enhancing mechanical property in ultra-high performance concrete by steel-fiber@ nano-silica. *Construction and Building Materials, 342*, 128069. https://doi.org/10.1016/j.conbuildmat.2022.128069

Iizuka, R., Yagi, T., Komatsu, K., Gotou, H., Tsuchiya, T., Kusaba, K., & Kagi, H. (2013). Crystal structure of the high-pressure phase of calcium hydroxide, portlandite: In situ powder and single-crystal X-ray diffraction study. *American Mineralogist, 98*, 1421–1428. https://doi.org/10.2138/am.2013.4386

Kanagaraj, B., Nammalvar, A., Andrushia, A. D., Gurupatham, B. G. A., & Roy, K. (2023). Influence of nano composites on the impact resistance of concrete at elevated temperatures. *Fire, 6*, 135. https://doi.org/10.3390/fire6040135

Khaloo, A., Mobini, M. H., & Hosseini, P. (2016). Influence of different types of nano-SiO_2 particles on properties of high-performance concrete. *Construction and Building Materials, 113*, 188–201. https://doi.org/10.1016/j.conbuildmat.2016.03.041

Khan, K., Ahmad, W., Amin, M. N., & Nazar, S. (2022a). Nano-silica-modified concrete: A bibliographic analysis and comprehensive review of material properties. *Nanomaterials, 12*, 1989. https://doi.org/10.3390/nano12121989

Khan, M., Cao, M., Chaopeng, X., & Ali, M. (2022b). Experimental and analytical study of hybrid fiber reinforced concrete prepared with basalt fiber under high temperature. *Fire and Materials, 46*, 205–226. https://doi.org/10.1002/fam.2968

Mahapatra, C. K., & Barai, S. V. (2019). Temperature impact on residual properties of self-compacting based hybrid fiber reinforced concrete with fly ash and colloidal nano silica. *Construction and Building Materials, 198*, 120–132. https://doi.org/10.1016/j.conbuildmat.2018.11.155

Mansourghanaei, M., Biklaryan, M., & Mardookhpour, A. (2022). Comparison of ultrasonic pulse passage velocity, in high-strength concrete and ordinary concrete, under high temperature based on XRD and SEM test, for use in pavement. *Journal of Transportation Research*. https://doi.org/10.22075/jtie.2022.25524.1577

Mazloom, M., Pourhaji, P., & Afzali-Naniz, O. (2021). Effects of halloysite nanotube, nano-silica and micro-silica on rheology, hardened properties and fracture energy of SCLC. *Structural Engineering and Mechanics, an Int'l Journal, 80*, 91–101. https://doi.org/10.12989/sem.2021.80.1.091

Merlino, S., Bonaccorsi, E., & Armbruster, T. (2000). The real structures of clinotobermorite and tobermorite 9 A: OD character, polytypes, and structural relationships. *European Journal of Mineralogy, 12*, 411–429. https://doi.org/10.1127/0935-1221/2000/0001-0411

Moore, D. M., & Reynolds, R. C. (1997). *X-ray diffraction and the identification and analysis of clay minerals*. Oxford University Press. https://doi.org/10.1017/S0016756898501501

Mukharjee, B. B., & Barai, S. V. (2014). Influence of nano-silica on the properties of recycled aggregate concrete. *Construction and Building Materials, 55*, 29–37. https://doi.org/10.1016/j.conbuildmat.2014.01.003

Mukharjee, B. B., & Barai, S. V. (2020). Influence of incorporation of colloidal nano-silica on behaviour of concrete. *Iranian Journal of Science and Technology, Transactions of Civil Engineering, 44*, 657–668. https://doi.org/10.1007/s40996-020-00382-0

Najeeb, Z., & Mosaberpanah, M. A. (2023). Mechanical and durability properties of modified high-performance mortar by using cenospheres and nano-silica. *Construction and Building Materials, 362*, 129782. https://doi.org/10.1016/j.conbuildmat.2022.129782

Nithurshan, M., Elakneswaran, Y., Yoda, Y., Kitagaki, R., & Hiroyoshi, N. (2024). Multiscale computational modelling of nano-silica reinforced cement paste: Bridging microstructure and mechanical performance. *Construction and Building Materials, 425*, 136047. https://doi.org/10.1016/j.conbuildmat.2024.136047

Ouhadi, V., & Yong, R. (2003). Impact of clay microstructure and mass absorption coefficient on the quantitative mineral identification by XRD analysis.

Applied Clay Science, 23, 141–148. https://doi.org/10.1016/S0169-1317(03)00096-6

Paul Thanaraj, D., Kiran, T., Kanagaraj, B., Nammalvar, A., Andrushia, A. D., Gurupatham, B. G. A., & Roy, K. (2023). Influence of heating-cooling regime on the engineering properties of structural concrete subjected to elevated temperature. *Buildings, 13*, 295. https://doi.org/10.3390/buildings13020295

Peng, G.-F., & Huang, Z.-S. (2008). Change in microstructure of hardened cement paste subjected to elevated temperatures. *Construction and Building Materials, 22*, 593–599. https://doi.org/10.1016/j.conbuildmat.2006.11.002

Raheem, A., Abdulwahab, R., & Kareem, M. (2021). Incorporation of metakaolin and nanosilica in blended cement mortar and concrete—A review. *Journal of Cleaner Production, 290*, 125852. https://doi.org/10.1016/j.jclepro.2021.125852

Rajamony Laila, L., Gurupatham, B. G. A., Roy, K., & Lim, J. B. P. (2021). Effect of super absorbent polymer on microstructural and mechanical properties of concrete blends using granite pulver. *Structural Concrete, 22*, E898–E915. https://doi.org/10.1002/suco.201900419

Rodriguez, E. T., Garbev, K., Merz, D., Black, L., & Richardson, I. G. (2017). Thermal stability of CSH phases and applicability of Richardson and Groves' and Richardson C-(A)-SH (I) models to synthetic CSH. *Cement and Concrete Research, 93*, 45–56. https://doi.org/10.1016/j.cemconres.2016.12.005

Rodriguez-Navarro, C., Ruiz-Agudo, E., Luque, A., Rodriguez-Navarro, A. B., & Ortega-Huertas, M. (2009). Thermal decomposition of calcite: Mechanisms of formation and textural evolution of CaO nanocrystals. *American Mineralogist, 94*, 578–593. https://doi.org/10.2138/am.2009.3021

Rosa, A., El-Barbary, A., Heggie, M., & Briddon, P. (2005). Structural and thermodynamic properties of water related defects in α-quartz. *Physics and Chemistry of Minerals, 32*, 323–331. https://doi.org/10.1007/s00269-005-0005-6

Sabeur, H., Platret, G., & Vincent, J. (2016). Composition and microstructural changes in an aged cement pastes upon two heating–cooling regimes, as studied by thermal analysis and X-ray diffraction. *Journal of Thermal Analysis and Calorimetry, 126*, 1023–1043. https://doi.org/10.1007/s10973-016-5639-8

Sadrmomtazi, A., Gashti, S. H., & Tahmouresi, B. (2020). Residual strength and microstructure of fiber reinforced self-compacting concrete exposed to high temperatures. *Construction and Building Materials, 230*, 116969. https://doi.org/10.1016/j.conbuildmat.2019.116969

Shyamala, G., Hemalatha, B., Devarajan, Y., Lakshmi, C., Munuswamy, D. B., & Kaliappan, N. (2023). Experimental investigation on the effect of nano-silica on reinforced concrete beam-column connection subjected to cyclic loading. *Scientific Reports, 13*, 17392. https://doi.org/10.1038/s41598-023-43882-5

Singh, H., Tiwary, A. K., & Singh, S. (2023). Experimental investigation on the performance of ground granulated blast furnace slag and nano-silica blended concrete exposed to elevated temperature. *Construction and Building Materials, 394*, 132088. https://doi.org/10.1016/j.conbuildmat.2023.132088

Sivakumar, N., & Ananthi, G. B. G. (2024). Characterisation of domestically discarded vegetable waste biomass ash and silica sand mixed with ordinary Portland cement concrete. *Biomass Conversion and Biorefinery*. https://doi.org/10.1007/s13399-024-05363-1

Tantawy, M. (2017). Effect of high temperatures on the microstructure of cement paste. *Journal of Materials Science and Chemical Engineering, 5*, 33. https://doi.org/10.4236/msce.2017.511004

Wang, J., Xie, Y., Zhong, X., & Feng, Z. (2022). Surface drying characteristic of early-age concrete considering cement hydration process. *Drying Technology, 40*, 3084–3099. https://doi.org/10.1080/07373937.2022.2047715

Yonggui, W., Shuaipeng, L., Hughes, P., & Yuhui, F. (2020). Mechanical properties and microstructure of basalt fibre and nano-silica reinforced recycled concrete after exposure to elevated temperatures. *Construction and Building Materials, 247*, 118561. https://doi.org/10.1016/j.conbuildmat.2020.118561

Zhang, P., Han, X., Guo, J., & Hu, S. (2023). High-temperature behavior of geopolymer mortar containing nano-silica. *Construction and Building Materials, 364*, 129983. https://doi.org/10.1016/j.conbuildmat.2021.122347

Publisher's Note

Motahereh Nasehi Ghashouieh Ph.D. Candidate in Department of Civil Engineering, Sirjan Branch, Islamic Azad University, Sirjan, Iran.

Mohsen Malekinejad Assistant Professor in Department of Civil Engineering, Sirjan Branch, Islamic Azad University, Sirjan, Iran.

Mohammad Amiri Associate professor in Faculty of Engineering, University of Hormozgan, Bandar Abbas, Iran.